SISSA

Design and construction of a new detector to measure ultra-low radioactive-isotope contamination of argon

View the article online for updates and enhancements.

IOP ebooks™

Bringing together innovative digital publishing with leading authors from the global scientific community.

Start exploring the collection−download the first chapter of every title for free.

Design and construction of a new detector to measure ultra-low radioactive-isotope contamination of argon

The DarkSide-20k collaboration

C.E. Aalseth,[a] S. Abdelhakim,[b] F. Acerbi,[c,d] P. Agnes,[e] R. Ajaj,[f] I.F.M. Albuquerque,[g]
T. Alexander,[a] A. Alici,[h,i] A.K. Alton,[j] P. Amaudruz,[k] F. Ameli,[l] J. Anstey,[f] P. Antonioli,[i]
M. Arba,[m] S. Arcelli,[h,i] R. Ardito,[n,o] I.J. Arnquist,[a] P. Arpaia,[p,q] D.M. Asner,[r] A. Asunskis,[s]
M. Ave,[g] H.O. Back,[a] V. Barbaryan,[t] A. Barrado Olmedo,[u] G. Batignani,[v,w] M.G. Bisogni,[v,w]
V. Bocci,[l] A. Bondar,[x,y] G. Bonfini,[z] W. Bonivento,[m] E. Borisova,[x,y] B. Bottino,[aa,ab]
M.G. Boulay,[f] R. Bunker,[a] S. Bussino,[ac,ad] A. Buzulutskov,[x,y] M. Cadeddu,[ae,m]
M. Cadoni,[ae,m] A. Caminata,[ab] N. Canci,[e,z] A. Candela,[z] C. Cantini,[af] M. Caravati,[m]
M. Cariello,[ab] F. Carnesecchi,[h,i,ag] M. Carpinelli,[ah,ai] A. Castellani,[n,o] P. Castello,[aj,m]
S. Catalanotti,[ak,q] V. Cataudella,[ak,q] P. Cavalcante,[al,z] D. Cavazza,[i] S. Cavuoti,[ak,q]
S. Cebrian,[am] J.M. Cela Ruiz,[u] B. Celano,[q] R. Cereseto,[ab] W. Cheng,[an,ao] A. Chepurnov,[t]
C. Cicalò,[m] L. Cifarelli,[h,i] M. Citterio,[o] F. Coccetti,[ag] A.G. Cocco,[q] V. Cocco,[m] M. Colocci,[h,i]
L. Consiglio,[ap] F. Cossio,[an,ao] G. Covone,[ak,q] P. Crivelli,[af] I. D'Antone,[i] M. D'Incecco,[z]
D. D'Urso,[ah,ai] M.D. Da Rocha Rolo,[an] O. Dadoun,[aq] M. Daniel,[u] S. Davini,[ab]
A. De Candia,[ak,q] S. De Cecco,[l,ar] M. De Deo,[z] A. De Falco,[m,ae] G. De Filippis,[ak,q]
D. De Gruttola,[as,ag] G. De Guido,[at,o] G. De Rosa,[ak,q] G. Dellacasa,[an] P. Demontis,[ah,ai,au]
S. DePaquale,[as] A.V. Derbin,[av] A. Devoto,[ae,m] F. Di Eusanio,[aw,z] L. Di Noto,[aa,ab]
G. Di Pietro,[z,o] P. Di Stefano,[ax] C. Dionisi,[l,ar] G. Dolganov,[ay] F. Dordei,[m] M. Downing,[az]
F. Edalatfar,[k] A. Empl,[e] M. Fernandez Diaz,[u] A. Ferri,[c,d] C. Filip,[ba] G. Fiorillo,[ak,q]
K. Fomenko,[bb] A. Franceschi,[bc] D. Franco,[bd] G.E. Froudakis,[be] F. Gabriele,[z] A. Gabrieli,[ah,ai]
C. Galbiati,[aw,ap] M. Garbini,[i,ag] P. Garcia Abia,[u] D. Gascón Fora,[bf] A. Gendotti,[af]
C. Ghiano,[z] A. Ghisi,[n,o] S. Giagu,[l,ar] P. Giampa,[k] R.A. Giampaolo,[an,ao] C. Giganti,[aq]
M.A. Giorgi,[w,v] G.K. Giovanetti,[aw] M.L. Gligan,[ba] A. Gola,[c,d] O. Gorchakov,[bb] M. Grab,[bg]
R. Graciani Diaz,[bf] F. Granato,[bh] M. Grassi,[v] J.W. Grate,[a] G.Y. Grigoriev,[ay] A. Grobov,[ay,bi]
M. Gromov,[t] M. Guan,[bj] M.B.B. Guerra,[s] M. Guerzoni,[i] M. Gulino,[bk,ai] R.K. Haaland,[bl]
B.R. Hackett,[bm] A. Hallin,[bn] B. Harrop,[aw] E.W. Hoppe,[a] S. Horikawa,[ap,z] B. Hosseini,[m]

F. Hubaut,^{bo} P. Humble,^{a} E.V. Hungerford,^{e} An. Ianni,^{aw,z} A. Ilyasov,^{ay,bi} V. Ippolito,^{l}
C. Jillings,^{bp,bq} K. Keeter,^{s} C.L. Kendziora,^{br} S. Kim,^{bh} I. Kochanek,^{z} K. Kondo,^{ap}
G. Kopp,^{aw} D. Korablev,^{bb} G. Korga,^{e,z} A. Kubankin,^{bs} R. Kugathasan,^{an,ao} M. Kuss,^{v}
M. Kuźniak,^{f,bt} M. La Commara,^{bu,q} L. La Delfa,^{m} M. Lai,^{ae,m} S. Langrock,^{bp} M. Lebois,^{b}
B. Lehnert,^{bn} N. Levashko,^{ay,bi} X. Li,^{aw} Q. Liqiang,^{b} M. Lissia,^{m} G.U. Lodi,^{at,o} G. Longo,^{ak,q}
R. López Manzano,^{u} R. Lussana,^{bv,o} L. Luzzi,^{bw,o} A.A. Machado,^{bx} I.N. Machulin,^{ay,bi}
A. Mandarano,^{ap,z} L. Mapelli,^{aw} M. Marcante,^{by,d,c} A. Margotti,^{i} S.M. Mari,^{ac,ad}
M. Mariani,^{bw,o} J. Maricic,^{bm} M. Marinelli,^{aa,ab} D. Marras,^{m} M. Martínez,^{am,bz}
J.J. Martínez Morales,^{u} A.D. Martinez Rojas,^{an,ao} C.J. Martoff,^{bh} M. Mascia,^{ca,m} J. Mason,^{f}
A. Masoni,^{m} A. Mazzi,^{c,d} A.B. McDonald,^{ax} A. Messina,^{l,ar} P.D. Meyers,^{aw} T. Miletic,^{bm}
R. Milincic,^{bm} A. Moggi,^{v} S. Moioli,^{at,o} J. Monroe,^{cb} M. Morrocchi,^{v} T. Mroz,^{bg} W. Mu,^{af}
V.N. Muratova,^{av} S. Murphy,^{af} C. Muscas,^{aj,m} P. Musico,^{ab} R. Nania,^{i} T. Napolitano,^{bc}
A. Navrer Agasson,^{aq} M. Nessi,^{cc} I. Nikulin,^{bs} A. Oleinik,^{bs} V. Oleynikov,^{x,y} M. Orsini,^{z}
F. Ortica,^{cd,ce} L. Pagani,^{cf} M. Pallavicini,^{aa,ab} S. Palmas,^{ca,m} L. Pandola,^{ai} E. Pantic,^{cf}
E. Paoloni,^{v,w} G. Paternoster,^{c,d} F. Pazzona,^{ah,ai} S. Peeters,^{cg} P.A. Pegoraro,^{aj,m} K. Pelczar,^{z}
L.A. Pellegrini,^{at,o} C. Pellegrino,^{i,ag} N. Pelliccia,^{cd,ce} F. Perotti,^{n,o} V. Pesudo,^{u} E. Picciau,^{ae,m}
C. Piemonte,^{c,d} F. Pietropaolo,^{cc} A. Pocar,^{az} T.R. Pollmann,^{ch} D. Portaluppi,^{bv,o}
S.S. Poudel,^{e} P. Pralavorio,^{bo} D. Price,^{ci} B. Radics,^{af} F. Raffaelli,^{v} F. Ragusa,^{cj,o} M. Razeti,^{m}
A. Razeto,^{z} V. Regazzoni,^{by,d,c} C. Regenfus,^{af} A.L. Renshaw,^{e} S. Rescia,^{r} M. Rescigno,^{l}
F. Retiere,^{k} L.P. Rignanese,^{h,i,ag} A. Rivetti,^{an} A. Romani,^{cd,ce} L. Romero,^{u} N. Rossi,^{l,z}
A. Rubbia,^{af} D. Sablone,^{bh,z} P. Sala,^{cc} P. Salatino,^{ck,q} O. Samoylov,^{bb} E. Sánchez García,^{u,1}
S. Sanfilippo,^{ad,ac} M. Sant,^{ah,ai} D. Santone,^{cb} R. Santorelli,^{u} C. Savarese,^{aw} E. Scapparone,^{i}
B. Schlitzer,^{cf} G. Scioli,^{h,i} E. Segreto,^{bx} A. Seifert,^{a} D.A. Semenov,^{av} A. Shchagin,^{bs}
A. Sheshukov,^{bb} S. Siddhanta,^{m} M. Simeone,^{ck,q} P.N. Singh,^{e} P. Skensved,^{ax}
M.D. Skorokhvatov,^{ay,bi} O. Smirnov,^{bb} G. Sobrero,^{ab} A. Sokolov,^{x,y} A. Sotnikov,^{bb}
R. Stainforth,^{f} A. Steri,^{m} S. Stracka,^{v} V. Strickland,^{f} G.B. Suffritti,^{ah,ai,au} S. Sulis,^{aj,m}
Y. Suvorov,^{ak,q,ay} A.M. Szelc,^{ci} R. Tartaglia,^{z} G. Testera,^{ab} T. Thorpe,^{ap,z} A. Tonazzo,^{bd}
A. Tosi,^{bv,o} M. Tuveri,^{m} E.V. Unzhakov,^{av} G. Usai,^{m,ae} A. Vacca,^{ca,m} E. Vázquez-Jáuregui,^{cl}
M. Verducci,^{l,ar} T. Viant,^{af} S. Viel,^{f} F. Villa,^{bv,o} A. Vishneva,^{bb} R.B. Vogelaar,^{al} M. Wada,^{m,bt}
J. Wahl,^{a} J.J. Walding,^{cb} H. Wang,^{cm} Y. Wang,^{cm} S. Westerdale,^{f} R.J. Wheadon,^{an}
R. Williams,^{a} J. Wilson,^{b} Marcin Wojcik,^{bg} Mariusz Wojcik,^{cn} S. Wu,^{af} X. Xiao,^{cm} C. Yang,^{bj}
Z. Ye,^{e} M. Zuffa^i and G. Zuzel^{bg}

^{a}*Pacific Northwest National Laboratory, Richland, WA 99352, U.S.A.*

^{b}*Institut de Physique Nuclèaire d'Orsay, Orsay 91406, France*

^{c}*Fondazione Bruno Kessler, Povo 38123, Italy*

^{d}*Trento Institute for Fundamental Physics and Applications, Povo 38123, Italy*

^{e}*Department of Physics, University of Houston, Houston, TX 77204, U.S.A.*

^{f}*Department of Physics, Carleton University, Ottawa, ON K1S 5B6, Canada*

^{g}*Instituto de Física, Universidade de São Paulo, São Paulo 05508-090, Brazil*

^{h}*Physics Department, Università degli Studi di Bologna, Bologna 40126, Italy*

^{i}*INFN Bologna, Bologna 40126, Italy*

---

^{1}Corresponding author.

[j] *Physics Department, Augustana University, Sioux Falls, SD 57197, U.S.A.*

[k] *TRIUMF, 4004 Wesbrook Mall, Vancouver, BC V6T 2A3, Canada*

[l] *INFN Sezione di Roma, Roma 00185, Italy*

[m] *INFN Cagliari, Cagliari 09042, Italy*

[n] *Civil and Environmental Engineering Department, Politecnico di Milano, Milano 20133, Italy*

[o] *INFN Milano, Milano 20133, Italy*

[p] *Department of Electrical Engineering and Information Technology,*
Università degli Studi "Federico II" di Napoli, Napoli 80125, Italy

[q] *INFN Napoli, Napoli 80126, Italy*

[r] *Brookhaven National Laboratory, Upton, NY 11973, U.S.A.*

[s] *School of Natural Sciences, Black Hills State University, Spearfish, SD 57799, U.S.A.*

[t] *Skobeltsyn Institute of Nuclear Physics, Lomonosov Moscow State University, Moscow 119234, Russia*

[u] *CIEMAT, Centro de Investigaciones Energéticas, Medioambientales y Tecnológicas, Madrid 28040, Spain*

[v] *INFN Pisa, Pisa 56127, Italy*

[w] *Physics Department, Università degli Studi di Pisa, Pisa 56127, Italy*

[x] *Budker Institute of Nuclear Physics, Novosibirsk 630090, Russia*

[y] *Novosibirsk State University, Novosibirsk 630090, Russia*

[z] *INFN Laboratori Nazionali del Gran Sasso, Assergi, L'Aquila 67100, Italy*

[aa] *Physics Department, Università degli Studi di Genova, Genova 16146, Italy*

[ab] *INFN Genova, Genova 16146, Italy*

[ac] *INFN Roma Tre, Roma 00146, Italy*

[ad] *Mathematics and Physics Department, Università degli Studi Roma Tre, Roma 00146, Italy*

[ae] *Physics Department, Università degli Studi di Cagliari, Cagliari 09042, Italy*

[af] *Institute for Particle Physics, ETH Zürich, Zürich 8093, Switzerland*

[ag] *Museo della fisica e Centro studi e Ricerche Enrico Fermi, Roma 00184, Italy*

[ah] *Chemistry and Pharmacy Department, Università degli Studi di Sassari, Sassari 07100, Italy*

[ai] *INFN Laboratori Nazionali del Sud, Catania 95123, Italy*

[aj] *Department of Electrical and Electronic Engineering, Università degli Studi, Cagliari 09023, Italy*

[ak] *Physics Department, Università degli Studi "Federico II" di Napoli, Napoli 80126, Italy*

[al] *Virginia Tech, Blacksburg, VA 24061, U.S.A.*

[am] *Centro de Astropartículas y Física de Altas Energías, Universidad de Zaragoza, Zaragoza 50009, Spain*

[an] *INFN Torino, Torino 10125, Italy*

[ao] *Department of Electronics and Communications, Politecnico di Torino, Torino 10129, Italy*

[ap] *Gran Sasso Science Institute, L'Aquila 67100, Italy*

[aq] *LPNHE, CNRS/IN2P3, Sorbonne Université, Université Paris Diderot, Paris 75252, France*

[ar] *Physics Department, Sapienza Università di Roma, Roma 00185, Italy*

[as] *INFN Salerno, Salerno 84084, Italy*

[at] *Chemistry, Materials and Chemical Engineering Department "G. Natta", Politecnico di Milano,*
Milano 20133, Italy

[au] *Interuniversity Consortium for Science and Technology of Materials, Firenze 50121, Italy*

[av] *Saint Petersburg Nuclear Physics Institute, Gatchina 188350, Russia*

[aw] *Physics Department, Princeton University, Princeton, NJ 08544, U.S.A.*

[ax] *Department of Physics, Engineering Physics and Astronomy, Queen's University,*
Kingston, ON K7L 3N6, Canada

[ay] National Research Centre Kurchatov Institute, Moscow 123182, Russia

[az] Amherst Center for Fundamental Interactions and Physics Department, University of Massachusetts, Amherst, MA 01003, U.S.A.

[ba] National Institute for R&D of Isotopic and Molecular Technologies, Cluj-Napoca 400293, Romania

[bb] Joint Institute for Nuclear Research, Dubna 141980, Russia

[bc] INFN Laboratori Nazionali di Frascati, Frascati 00044, Italy

[bd] APC, Université Paris Diderot, CNRS/IN2P3, CEA/Irfu, Obs de Paris, USPC, Paris 75205, France

[be] Department of Chemistry, University of Crete, P.O. Box 2208, Heraklion 71003, Crete, Greece

[bf] Universiatat de Barcelona, Barcelona E-08028, Catalonia, Spain

[bg] M. Smoluchowski Institute of Physics, Jagiellonian University, Krakow 30-348, Poland

[bh] Physics Department, Temple University, Philadelphia, PA 19122, U.S.A.

[bi] National Research Nuclear University MEPhI, Moscow 115409, Russia

[bj] Institute of High Energy Physics, Beijing 100049, China

[bk] Engineering and Architecture Faculty, Università di Enna Kore, Enna 94100, Italy

[bl] Department of Physics and Engineering, Fort Lewis College, Durango, CO 81301, U.S.A.

[bm] Department of Physics and Astronomy, University of Hawai'i, Honolulu, HI 96822, U.S.A.

[bn] Department of Physics, University of Alberta, Edmonton, AB T6G 2R3, Canada

[bo] Centre de Physique des Particules de Marseille, Aix Marseille Univ, CNRS/IN2P3, CPPM, Marseille, France

[bp] Department of Physics and Astronomy, Laurentian University, Sudbury, ON P3E 2C6, Canada

[bq] SNOLAB, Lively, ON P3Y 1N2, Canada

[br] Fermi National Accelerator Laboratory, Batavia, IL 60510, U.S.A.

[bs] Radiation Physics Laboratory, Belgorod National Research University, Belgorod 308007, Russia

[bt] AstroCeNT, Nicolaus Copernicus Astronomical Center, Polish Academy of Sciences, Rektorska 4, Warsaw 00-614, Poland

[bu] Pharmacy Department, Università degli Studi "Federico II" di Napoli, Napoli 80131, Italy

[bv] Electronics, Information, and Bioengineering Department, Politecnico di Milano, Milano 20133, Italy

[bw] Energy Department, Politecnico di Milano, Milano 20133, Italy

[bx] Physics Institute, Universidade Estadual de Campinas, Campinas 13083, Brazil

[by] Physics Department, Università degli Studi di Trento, Povo 38123, Italy

[bz] ARAID, Fundación Agencia Aragonesa para la Investigación y el Desarrollo, Gobierno de Aragón, Zaragoza 50018, Spain

[ca] Department of Mechanical, Chemical, and Materials Engineering, Università degli Studi, Cagliari 09042, Italy

[cb] Department of Physics, Royal Holloway University of London, Egham TW20 0EX, U.K.

[cc] CERN, European Organization for Nuclear Research, CERN, Geneve 23 1211, Switzerland

[cd] Chemistry, Biology and Biotechnology Department, Università degli Studi di Perugia, Perugia 06123, Italy

[ce] INFN Perugia, Perugia 06123, Italy

[cf] Department of Physics, University of California, Davis, CA 95616, U.S.A.

[cg] Physics and Astronomy, University of Sussex, Brighton BN1 9QH, U.K.

[ch] Physik Department, Technische Universität München, Munich 80333, Germany

[ci] The University of Manchester, Manchester M13 9PL, United Kingdom

[cj] Physics Department, Università degli Studi di Milano, Milano 20133, Italy

^{ck}*Chemical, Materials, and Industrial Production Engineering Department,*
Università degli Studi "Federico II" di Napoli, Napoli 80126, Italy

^{cl}*Instituto de Física, Universidad Nacional Autónoma de México (UNAM), Ciudad de México 01000, Mexico*

^{cm}*Physics and Astronomy Department, University of California, Los Angeles, CA 90095, U.S.A.*

^{cn}*Institute of Applied Radiation Chemistry, Lodz University of Technology, 93-590 Lodz, Poland*

E-mail: ds-ed@lngs.infn.it

ABSTRACT: Large liquid argon detectors offer one of the best avenues for the detection of galactic weakly interacting massive particles (WIMPs) via their scattering on atomic nuclei. The liquid argon target allows exquisite discrimination between nuclear and electron recoil signals via pulse-shape discrimination of the scintillation signals. Atmospheric argon (AAr), however, has a naturally occurring radioactive isotope, ^{39}Ar, a β emitter of cosmogenic origin. For large detectors, the atmospheric ^{39}Ar activity poses pile-up concerns. The use of argon extracted from underground wells, deprived of ^{39}Ar, is key to the physics potential of these experiments. The DarkSide-20k dark matter search experiment will operate a dual-phase time projection chamber with 50 tonnes of radio-pure underground argon (UAr), that was shown to be depleted of ^{39}Ar with respect to AAr by a factor larger than 1400. Assessing the ^{39}Ar content of the UAr during extraction is crucial for the success of DarkSide-20k, as well as for future experiments of the Global Argon Dark Matter Collaboration (GADMC). This will be carried out by the DArT in ArDM experiment, a small chamber made with extremely radio-pure materials that will be placed at the centre of the ArDM detector, in the Canfranc Underground Laboratory (LSC) in Spain. The ArDM LAr volume acts as an active veto for background radioactivity, mostly γ-rays from the ArDM detector materials and the surrounding rock. This article describes the DArT in ArDM project, including the chamber design and construction, and reviews the background required to achieve the expected performance of the detector.

Contents

1 Introduction

Dark matter has played a fundamental role in the evolution of the universe at a cosmological scale, having a measurable impact in its expansion rate, and significantly contributing to large-scale structure formation. Nowadays, dark matter accounts for around 27% of the energy-matter content of the universe. In spite of its abundance, what makes up the dark matter is yet to be understood. Many candidates have been hypothesized, ranging from the primordial black holes predicted by General Relativity, to Weakly Interacting Massive Particles, that are predicted by many theories beyond the Standard Model of particle physics. Direct observation of dark matter is a major objective in modern fundamental physics.

Experiments searching for WIMPs intend to detect them via the signals (ionization, scintillation, and heat) they might leave when they undergo elastic scattering off atomic nuclei. Noble elements, like xenon and argon, are ideal active targets, as they are bright scintillators. Environmental radioactivity can easily overwhelm WIMP signals if not carefully eliminated or discriminated against. The detection properties of liquid argon (LAr) are particularly favourable for the rejection of radioactive backgrounds that produce electron recoils (ERs). Indeed, there is significant difference between the time distribution of the scintillation signals produced by these interactions compared to that of nuclear recoil (NR) events. The DEAP-3600 experiment, with 3200 kg of LAr, has demonstrated an exceptional pulse shape discrimination (PSD) against such background, projected to be over 10^9 [1]. The DarkSide-50 experiment has demonstrated the background-free capability of the dual-phase time projection chamber technique, in which both the primary scintillation and the electroluminescence from electrons multiplied in a gaseous region above the liquid are detected [2]. This technique also provides excellent position reconstruction capability that enables efficient

fiducialization [3, 4]. Single- or dual-phase LAr TPC with pulse-shape discrimination provides excellent sensitivity to WIMP masses above ~30 GeV/c^2. The dual-phase method also allows to search for lighter WIMP (<10 GeV/c^2) using the electroluminescence signal alone, as demonstrated by DarkSide-50 [5, 6]. With careful control of ER background from local radioactivity and reduction of ^{39}Ar background, a 1 tonne LAr detector has the potential to reach the *neutrino floor* due to solar neutrino interactions, via coherent elastic scattering on target nuclei, in this low mass region.

Given the strong potential for the LAr technology to push the sensitivity for WIMP detection several orders of magnitude beyond current levels, scientists from ArDM, DarkSide-50, DEAP-3600, and MiniCLEAN have joined forces to found the Global Argon Dark Matter collaboration (GADMC) to pursue a sequence of future experiments that will exploit this technology, starting with DarkSide-20k. A potentially limiting factor for the sensitivity of LAr-based experiments is the presence of the ^{39}Ar radioactive isotope, present at a rate of 1 Bq/kg in atmospheric argon. One of the key enabling technologies of the GADMC program is the argon target obtained from the high-throughput extraction of low-radioactivity argon naturally depleted in ^{39}Ar from underground sources (UAr) via the Urania plant in Cortez (U.S.A.). Urania will deliver 330 kg/day of 99.99% purity UAr. The underground argon will be further chemically purified to detector-grade argon in Aria at the rate of 1 tonne/day. Aria is a 350 m cryogenic distillation plant currently being commissioned in Sardinia, Italy. Although not its primary goal, Aria can also be operated in isotope separation mode to achieve a 10-fold suppression of ^{39}Ar per pass at a rate of 10 kg/day.

The DArT in ArDM experiment at the Canfranc Underground Laboratory (LSC), Spain, will measure the ^{39}Ar content in batches of the UAr delivered by Urania and Aria. In the shielded environment of the LSC, DArT in ArDM will be sensitive to very high depletion factors of ^{39}Ar, of the order of 1000. These measurements are crucial for the DarkSide-20k physics program and for the future experiments of the Global Argon Dark Matter collaboration.

2 The DArT in ArDM experiment

The DArT in ArDM experiment at LSC aims at measuring UAr-to-AAr ^{39}Ar depletion factors of the order of 1000 with 10% precision in one week of running. The ^{39}Ar isotope decays via β emission with an end-point of 565 keV. DArT is a single-phase liquid argon detector, with an active volume of approximately one litre, that will be filled with underground argon samples from Aria. Sampling directly UAr from Urania, with a SAES getter in front, would also be possible. The light produced by ionizing radiation in the active volume will be readout by two 1 cm^2 silicon photo-multipliers (SiPMs) procured from the DarkSide-20k production packaged with the cryogenic readout electronics. DArT will be housed at the centre of the 1 tonne LAr ArDM detector [7, 8] (figure 1), which will serve as an active veto to tag both internal and external radiation. The ArDM setup will be operated in the single-phase mode with a new set of low-radioactivity photo-multipliers (PMTs), 6 at the top and 7 at the bottom. A reflector foil coated with TPB wavelength shifter will cover the inner surface of the cylindrical barrel to enhance light collection. The cryostat is surrounded by a 50 cm thick polyethylene shielding (not shown in the figure 1).

Background is largely composed of γ-rays originating from within the detector materials and from the surrounding cavern that are energetic enough to penetrate into the DArT chamber. To minimize the background induced by its intrinsic radioactivity, DArT is built with selected radio-
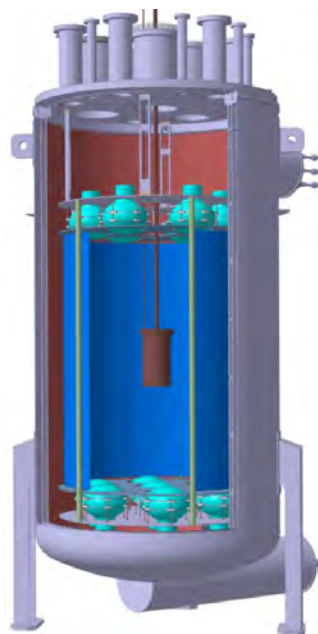
Figure 1. DArT detector in the centre of the ArDM cryostat.

pure materials. In DArT, the LAr is contained inside an outer vessel made of ultra-pure 99.99% Oxygen Free High Conductivity (OFHC) copper. A smaller cylindrical structure made of radio-pure acrylic (PMMA) is inserted in the copper cell and provides the cleanest possible surface for the UAr under test, as well as the support for the SiPM detector assemblies. Following a procedure developed by the DEAP-3600 collaboration [9], the inner surfaces of the acrylic structure directly in contact with the argon are sanded after fabrication to suppress backgrounds deriving from the plate-out of ^{222}Rn daughters.

In order to suppress the impact of external photons from the experimental cavern, which dominate the background budget, a 6 tonne lead shield will be installed around the ArDM vessel, in the hollow space between the ArDM cryostat and polyethylene shielding. The lead shield is a 140 cm height octagonal prism, with 10 cm width walls. In this configuration, the detector will be capable of measuring with high precision the larger ^{39}Ar depletion factors of the UAr batches coming from the Urania plant.

The lateral wall of the copper cylinder is 5 mm thick and the top and bottom caps are 8 mm thick (figure 2). The top flange allows access to the inner part of the chamber. A 1.5 mm thick indium wire is used to seal the top flange-copper cylinder interface. The contribution of indium to the overall background budget is negligible. The DArT instrumentation and services, including SiPM bias and readout, and a level meter signal, are routed through the top flange into a 15 cm long copper pipe leading to the top of the ArDM cryostat. A thinner off axis pipe, that penetrates the copper chamber and extends almost all the way to the bottom, is the argon fill line.

The inner acrylic structure is made of 8 pieces (figure 3): attachment to the top cover, inner and outer cylinders, 2 SiPM supports, 2 end caps, and facilities support on the bottom. Two 6 mm thick disks cap the inner cylinders in front of the SiPMs. The internal surfaces of these disks and the inner acrylic cylinder are coated with 200 μg/cm^2 wavelength shifter (TPB). The outer surface of

the acrylic is wrapped in Vikuiti reflector foil [10, 11]. An additional cylindrical shell (annulus) is used as a filler between the reflector foil and the copper vessel. The outer acrylic parts are attached to the top vessel flange. Two dedicated boards attached to the bottom and top acrylic disk with acrylic screws hold the SiPMs.
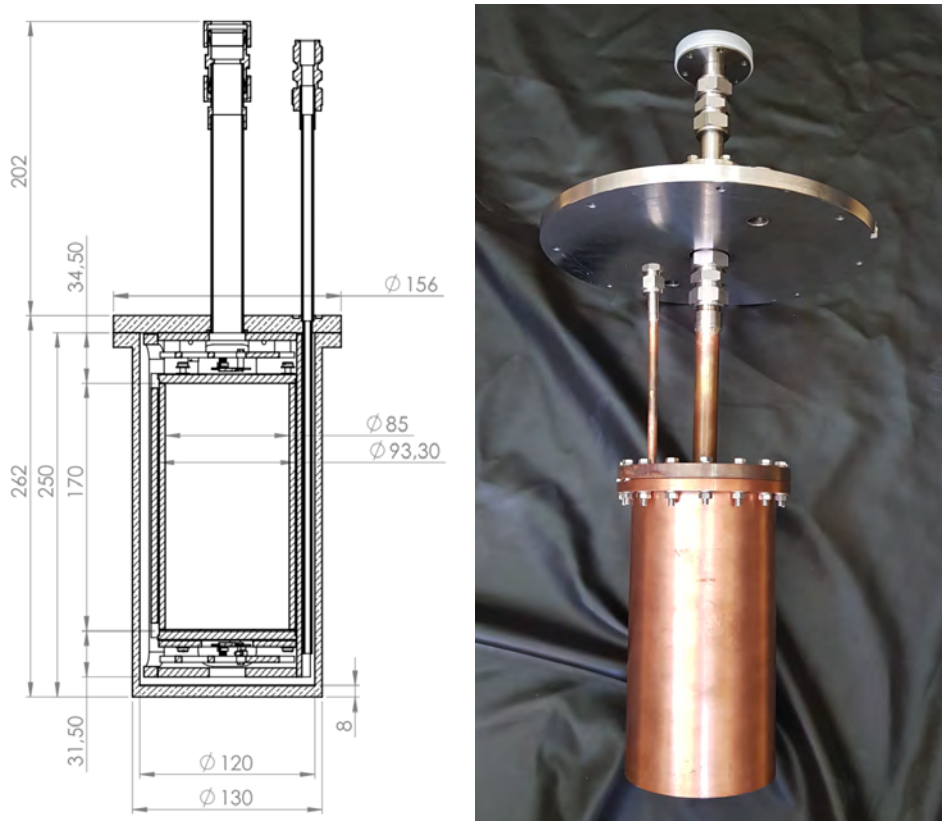

Figure 2. (Left) Sketch of the inner structure of DArT. (Right) Picture of the actual detector. The short stainless steel pipes are used in the cryogenic tests, and will be replaced by longer tubes in the final setup.

Currently in its construction phase, the DArT in ArDM experiment is expected to test UAr not only for DarkSide-20k, but also for any future experiment of the GADMC, such as ARGO [12] and a possible tonne-scale detector to search for light dark matter. It is also being considered for use by other experiments [13].

3   Cryogenics

DArT is connected to the cryogenic system of the experiment through two copper pipes (figure 2). They are joined with a silver brazing to two stainless steel pipes that go up to a CF200 flange, on top of ArDM, which provides the external connections. The schematics of the gas handling system and cryogenics is in figure 4. High oxygen traces in the liquid argon would quench the scintillation signal produced in the detector target. Hence, less than 1 ppm of oxygen is left in the chamber before filling it with argon, pumping the system below 10^{-3} mbar at room temperature. The pumping system is equipped with vacuum gauges and a turbo pump connected to valve V11.

Figure 3. (Left) Inner acrylic structure lateral view. (Right) Top acrylic cap and support disk with the photo-detector module installed.
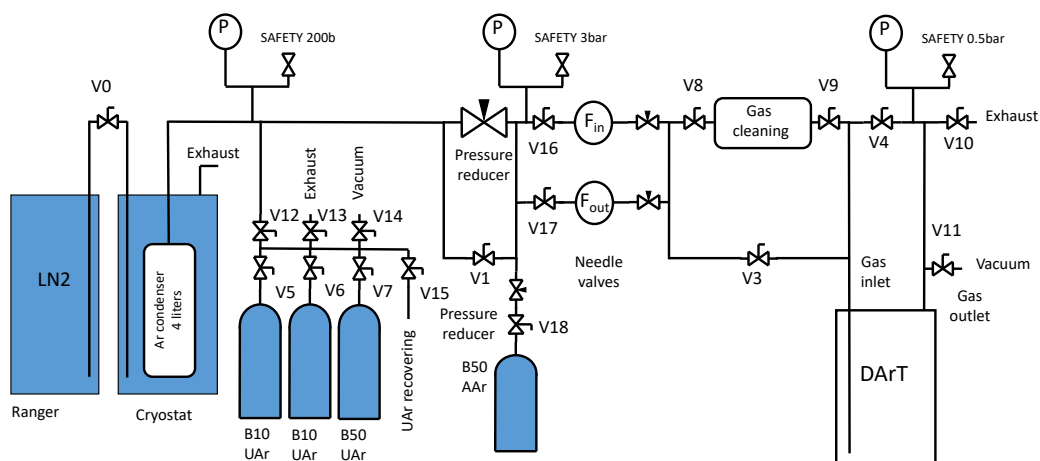

Figure 4. Schematics of the gas handling and cryogenic system for the operation of DArT. P indicates mechanical pressure gauges, F stands for flow meters and V denotes valves.

The pump is kept on while the system is warm. The system is proven leak tight at a level better than 10^{-7} mbar ℓ/s.

In normal operational conditions the DArT chamber is kept isolated closing all the in/out valves and reaches the thermal equilibrium with the surrounding liquid argon of ArDM. The pressure inside DArT is very close to the pressure of ArDM which, in order to avoid argon contamination in case of a small leak, is kept at a few mbar above the atmospheric pressure.

DArT will undergo filling and emptying cycles as needed for testing different argon batches. The evacuated DArT chamber is filled by condensing gaseous argon on the walls of the vessel (5 mm thick) and of the copper pipes (1 mm thick), whose external sides are maintained at fixed temperature by the ArDM LAr bath. The filling rate is established by the inflow meter/controller,

which supplies the STP argon gas to be cooled and condensed in DArT. Given the high thermal conductivity of copper, a substantial filling rate can be maintained without a significant drop of temperature across the copper walls and without a significant increment of the pressure inside DArT. The limiting factor for filling DArT is the ability of ArDM to dissipate safely to the cryocoolers the heat needed to condense the Ar. The ArDM dissipated heat is limited to a maximum of 20 W. The amount of LAr in DArT is 1.58 liters. To fill DArT, the energy needed for cooling the argon gas to its liquefaction point is 230 KJ, while 355 KJ are needed for its full condensation. The filling level of the DArT chamber is monitored by three PT1000 sensors. These platinum resistors are used as level sensors thanks to the different self-heating of their resistance in gas (with thermal conductance 3.2 mW/K) and liquid (32 mW/K) phases. When filling, the argon flows through a hot getter for its further purification before reaching the DArT chamber.

The time required for filling DArT is at least 8 hours. The expected run time of the experiment ranges from one to several weeks per argon batch, depending on the argon purity. Therefore, one full day for condensing and evaporating the argon in the chamber is not a dominant component in the duty cycle of the experiment.

To empty the DArT chamber, the argon is evaporated and temporarily stored in a 4 liter condenser bottle, enclosed in an LN_2 cryostat. As the condenser is refrigerated with liquid nitrogen (77 K), the argon converts into solid phase and therefore its saturated vapor pressure is about 260 mbar. This pressure cannot of course be applied directly to the liquid argon in the DArT chamber because the LAr would also freeze. The flow of gaseous argon into the condenser is therefore controlled in such a way that the pressure inside the DArT chamber is higher than the triple point pressure of LAr (682 mbar) and lower than the equilibrium pressure of ArDM. These operating conditions guarantee that neither the LAr will freeze within the DArT chamber nor the gaseous argon will re-condense on the walls on its way out. In particular, the LAr will become overheated and will evaporate on the free surface of the LAr, cooling a layer of liquid beneath the surface. Because of the low thermal conductivity of the LAr, the surface is thermally insulated from the bulk of LAr and the evaporation process is very inefficient. To speed up the evaporation of the LAr, two PT100 platinum resistors, dissipating 3.5 W each, are located near the bottom of the DArT chamber. The work required to evaporate the DArT LAr is 355 kJ, so the chamber is emptied in about 14 hours. When the DArT chamber is empty, the condenser will be full and it may be warmed up. The argon gas is then transferred to a high-pressure storage bottle.

4 Photo-electronics

Scintillation light in DArT will be collected by two photo-detector elements (PDE), specifically designed to maximise the radiopurity and simplify the connections. Each PDE (figure 5) is based on a module integrating both, a 11.9×7.8 mm^2 SiPM, and the readout electronics in a 15×26 mm^2 PCB. The SiPM cell size is 25 μm, and has quenching resistor of 10 MΩ at 77 K. These SiPMs are based on the NUV-HD-Cryo technology developed by FBK for DarkSide-20k, which allows low afterpulse at cryogenic temperature with extended over-voltage [14]. The SiPM sensitivity peaks at 400–420 nm, with a photo-detection efficiency above 50% at room temperature. The pre-amplifier is based on the low-noise design developed at LNGS [15]. Overall, a signal-to-noise ratio in excess of 40 is achieved when operated at an overvoltage of 7 V, with a rise time of 2 ns and a total power

dissipation of 200 mW. The dynamic range is measured in laboratory tests to be between 1.5 and 1000 photo-electrons (PE). An optical fiber routed inside the LAr chamber will carry LED pulses to be used to monitor the response and the stability of the SiPMs over time.

The energy scale of DArT will be studied with AAr, that provides a well-known, high statistics ^{39}Ar spectrum. The energy resolution will be measured using an ^{83m}Kr gaseous source injected into the argon stream, a method first demonstrated in argon in 2009 [16] and successfully exploited since then in many experiments, including DarkSide-50 [2, 17].
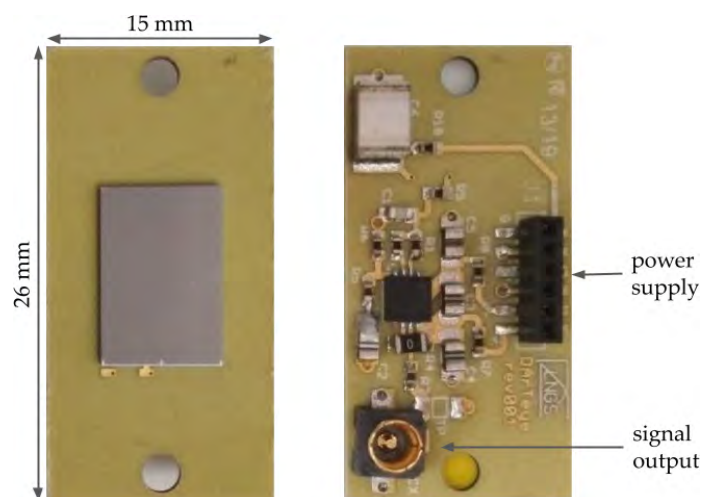
Figure 5. Images of the front and back sides of the front-end boards housing the SiPM for light readout.

5 Signal and background studies

In the DArT detector, signal events are electron recoils from the β decay of ^{39}Ar, which have an energy end-point of 565 keV occurring within the inner acrylic vessel. These events deposit all their energy in DArT, leaving no signal in the veto detector, ArDM. The range of the energy spectrum in DArT below 600 keV is defined as the *region of interest* (ROI) where the signal events are contained. Background events stem from radioactive decays in the detector materials and in the experimental hall surrounding the detector. They typically produce γ particles that deposit energy in DArT and/or in ArDM via Compton scattering. We assume that nuclear recoils are efficiently rejected using the powerful scintillation pulse shape discrimination technique in LAr. Background events that leave a signal with energy in the DArT ROI are tagged as background and removed from the analysis when they also deposit more than 10 keV in ArDM. If, however, less than 10 keV is deposited in ArDM they will go *untagged* and contribute to the background of the measurement.

The amount of ^{39}Ar in an argon sample is determined from fits to the spectral shapes of electron-like recoils in the LAr target with no coincident ArDM tag. The normalization of the background can be constrained by the high-energy region of the DArT energy spectrum, above 600 keV, where no signal events reside and whose rate is assumed constant or predictable in time.

Studies of the physics reach of the experiment are performed with tuned-on-data Monte Carlo simulations based on Geant4 [18], with the simulation framework of the DarkSide-50 experiment

(G4DS [17]). This package contains a detailed description of DArT and ArDM layout, including the lead and polyethylene shields. Predictions for the number of signal and background events expected in the ROI are based on these simulations. Background rates and origin are based on actual assays of screened materials and *in situ* measurements in the underground hall A at LSC. The values for the radio-impurities and masses of internal materials are summarized in table 1, along with the figures for the external background (from outside ArDM).

A study was conducted to assess the need for the lead shield. The total number of background events per week in the ROI with the lead shield is 7210, of which 465 are untagged. About 35% of the background comes from sources external to ArDM [19]. For comparison, the expected number of untagged background events in the ROI without the lead shield is 10300 out of 122000 total events (96% external background, see figure 6).
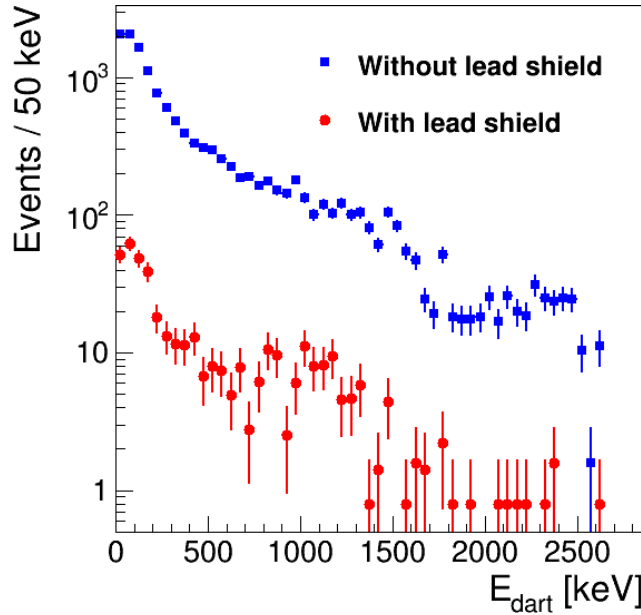
Figure 6. Expected untagged background events in DArT with the lead shield (red circles) and without (blue squares) in one month of data taking, assuming a veto threshold of 10 keV.

The DArT fiducial mass is 1.42 kg of LAr. Assuming the ^{39}Ar activity in the UAr measured by DarkSide-50 is 0.73 mBq/kg (for a corresponding depletion factor of 1400), we expect 631 signal events per week, yielding a signal-to-background ratio (S/B) of ≈ 0.06 without the lead shield. The lead shield reduces the external background by a factor ~ 20, leading to S/B ≈ 1.3.

The current ArDM single-phase geometry, with only 13 PMTs and DArT shading some of the light, will be able to detect events with energies as low as 10 keV. The sensitivity to the ^{39}Ar signal is subject to further optimisation by tuning the ArDM veto energy threshold. The dependence of the number of untagged background events in DArT is calculated as function of such threshold, and is found to be linear with a slope of 8.5×10^{-3}/keV.

6 Light response simulation

The energy deposits in the liquid argon of DArT produce vacuum ultraviolet photons (VUV) that, once converted to visible photons (420 nm) by the TPB, are either detected by the two SiPMs or

Table 1. Activities (in mBq/kg, except for ^{210}Bi that is in mBq/m^2), masses (kg) and surface areas (cm^2) for the different materials used for ArDM and DArT simulations. As the ^{238}U secular equilibrium in Arlon is broken, the upper, middle and lower parts of the chain are considered.

Source		^{238}U	^{232}Th	^{40}K	^{60}Co	^{210}Pb	^{210}Bi	mass [kg]
ArDM Cryo		3.42	6.37	1.3	11.21			1630
ArDM PMTs	Base	9176	11043	1978				10.8
	Metal	181	73	371				
	Glass	636	115	53	2			
Lead shield		0.37	0.073	0.31		10		6000
ArDM pillars		0.012	0.04	0.06	0.04			26.5
ArDM rings		3.42	6.37	1.3	11.21			4
PMTs support		3.42	6.37	1.3	11.21			16
Acrylic		0.004	0.005				0.22	1.8
DArT Cu		0.012	0.04	0.06	0.04			6.95
SiPM Arlon	Up	3.8						0.001
	Mid	53	70	1300				
	Low	137						
Solder brazing		1203	406	3090				0.001
External		0.72,*	0.13,*	0.05,*				800700,**

*γ flux per cm^2 at the outer surface of the polyethylene shielding of ArDM.
**Surface in cm^2.

absorbed elsewhere. The simulation of the propagation of photons to the SiPMs with Geant4 takes into account the optical properties of the detector materials and their interfaces, in particular the acrylic (PMMA), the TPB coating of the internal surfaces, the reflector foil and the SiPM planes. Most of these materials are modelled as pure dielectrics, with the exception of the reflector which is assumed metallic, i.e. a surface that photons cannot penetrate. The TPB is assumed to re-emit a single visible photon (VIS) for each absorbed VUV photon with a characteristic time of 1.5 ns. The SiPMs are modelled as dielectrics with an arbitrarily reduced absorption length, in order to fully absorb the transmitted visible photons in a few nanometers. Absorbed photons are converted to photo-electrons, with a photon detection efficiency (PDE) of 40%. Simulation parameters are tuned according to reference [17].

The light response of the detector is evaluated simulating 20000 ^{39}Ar events in the DArT active volume. The mean energy of the ^{39}Ar β emission is 210 keV. Thus, considering a w-value for producing a VUV scintillation photon in LAr of 19.5 eV, and a quenching factor of 0.95 for

electrons [20], on average 10230 photons are produced per event, corresponding to 48.7 VUV-photons keV. The fraction of visible photons produced per VUV photon is ~98.5%, which accounts for the tiny absorption of VUV photons in LAr.

The reflector foil is placed on the sides of the active volume and on the top and bottom acrylic caps, around the SiPMs, providing a light collection efficiency largely independent of the event position (figure 7). The average light collection efficiency is ~58%, which corresponds to a light yield of 11 PE/keV for 40% PDE. For reference, about 3000 PE are recorded per SiPM for energy deposits at the endpoint of the ^{39}Ar spectrum. Approximately, 30% of the scintillation photons are collected in ~4 ns (the fast component in Ar), that is ~900 PE, well within the dynamic range of the readout electronics. The slow scintillation component delivers photons over an extended period. If the dynamic range of the light sensors turns out to be insufficient, the LY can be decreased by reducing either the overvoltage of the SiPMs (that is related to the PDE) or the effective area of the reflector.

The energy resolution is calculated with energy deposits from 50 keV up to 800 keV uniformly distributed in the DArT active volume. An energy resolution between 3% and 6% is found in the ROI.
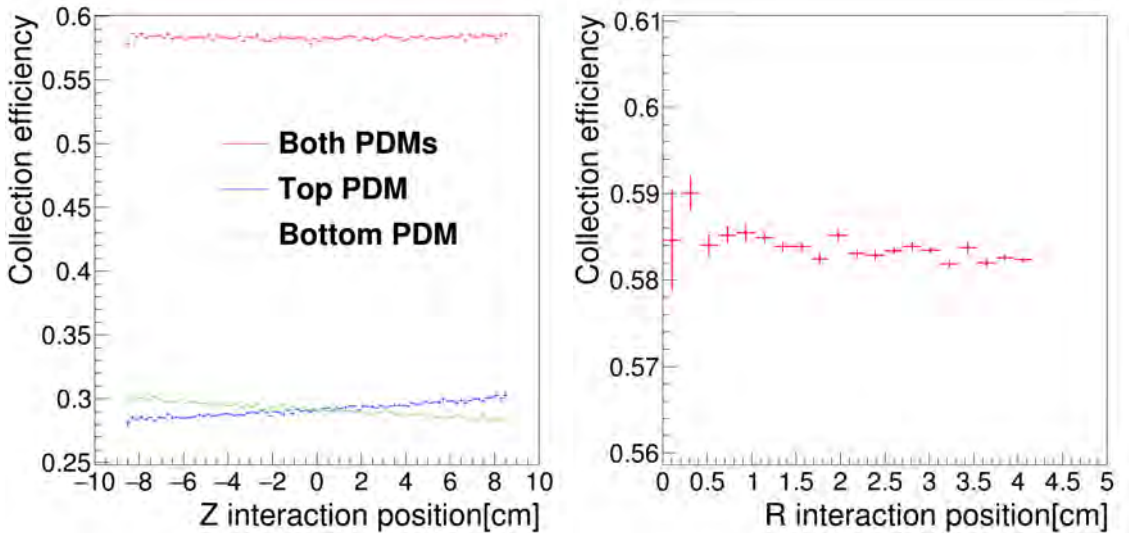
Figure 7. Average light collection efficiency vs. height (left) and radius (right) of the interaction position.

7 Sensitivity to the ^{39}Ar signal

Using the background values and the light characterization illustrated above, we evaluate the DArT sensitivity expected for different ^{39}Ar depletion factors, using a veto threshold of 10 keV. In the following, we calculate both the measurement uncertainty on the depletion factors in case a clear signal is observed and the 90% confidence level (C.L.) upper limits in absence of an excess over the expected background.

A typical photo-electron spectrum, for background and signal events acquired in one week of running of DArT, is displayed in figures 8 for ^{39}Ar depletion factors of 10 and 1400, respectively.

The so-called *simulated data* distribution is a randomized distribution generated from the sum of the signal and background distributions. The ^{39}Ar content is extracted from a fit of the observed shape to the weighted sum of the signal and background distributions. From these fits, the expected statistical uncertainties per week on the measurement of different depletion factors of ^{39}Ar are extracted. In the configuration with the lead shield, the uncertainty is below 1% for a depletion factor (DF) of 10, 1% for $DF = 100$, 7% for $DF = 1400$ and 40% for $DF = 14000$. The upper limit at the 90% C.L. is reached for $DF \approx 6 \times 10^4$. Without the lead shield, the statistical uncertainties increase, typically, by a factor 3, and the 90% C.L. upper limit is $DF \approx 5000$.
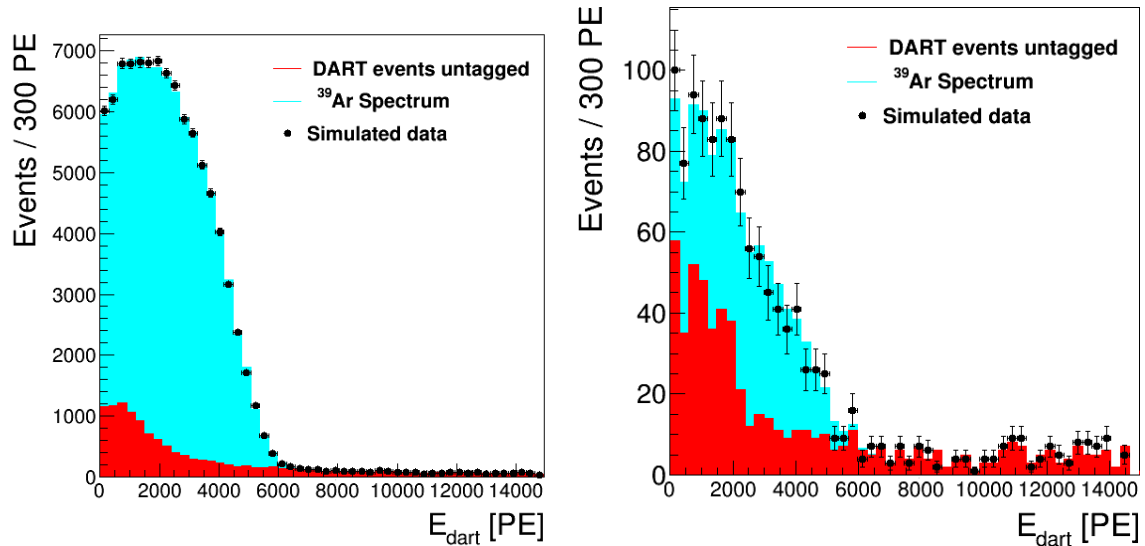
Figure 8. Photo-electron spectra corresponding to one week of data taking, (left) for an ^{39}Ar $DF = 10$ without lead shield and (right) for $DF = 1400$ with lead shield. The red (dark) histogram represents the background spectrum, the blue (light) histogram is the ^{39}Ar signal and the black dots denote the simulated data.

These results assume the knowledge of the spectral shape of the signal and background from the simulations and, therefore, do not include systematic uncertainties. Systematic uncertainties on the ^{39}Ar decay spectrum can be significantly reduced validating the simulated spectra with a large data sample in an AAr run.

The background shape in the ROI will also need to be validated with data. The analysis strategy envisaged is to start from the total measured background spectrum (before using the tagging cut) and then applying to it the veto cut efficiency vs. energy obtained from the simulations. From our relatively high threshold and detailed simulation studies, we are confident that the efficiency is high.

8   Conclusions

We have designed the DArT in ArDM experiment capable of measuring with high precision the amount of ^{39}Ar in the argon that will be used in current and future dark matter search experiments. The detector is under construction. The sensitivity of DArT in ArDM was studied using a detailed background model and light response simulations. These studies show that our detector will allow us to measure UAr depletion factors in excess of 1000 with statistical accuracy better than 10% in

one week of counting time. Dedicated studies of systematic uncertainties on the background shapes are underway.

Acknowledgments

References

[1] DEAP-3600 collaboration, *First results from the DEAP-3600 dark matter search with argon at SNOLAB*, *Phys. Rev. Lett.* **121** (2018) 071801 [arXiv:1707.08042].

[2] DARKSIDE collaboration, *DarkSide-50 532-day Dark Matter Search with Low-Radioactivity Argon*, *Phys. Rev.* **D 98** (2018) 102006 [arXiv:1802.07198].

[3] DARKSIDE collaboration, *First Results from the DarkSide-50 Dark Matter Experiment at Laboratori Nazionali del Gran Sasso*, *Phys. Lett.* **B 743** (2015) 456 [arXiv:1410.0653].

[4] DARKSIDE collaboration, *Results From the First Use of Low Radioactivity Argon in a Dark Matter Search*, *Phys. Rev.* **D 93** (2016) 081101 [arXiv:1510.00702].

[5] DARKSIDE collaboration, *Low-Mass Dark Matter Search with the DarkSide-50 Experiment*, *Phys. Rev. Lett.* **121** (2018) 081307 [arXiv:1802.06994].

[6] DARKSIDE collaboration, *Constraints on Sub-GeV Dark-Matter-Electron Scattering from the DarkSide-50 Experiment*, *Phys. Rev. Lett.* **121** (2018) 111303 [arXiv:1802.06998].

[7] ARDM collaboration, *ArDM: a ton-scale LAr detector for direct Dark Matter searches*, *J. Phys. Conf. Ser.* **308** (2011) 012006 [arXiv:1012.5967].

[8] ArDM collaboration, *Commissioning of the ArDM experiment at the Canfranc underground laboratory: first steps towards a tonne-scale liquid argon time projection chamber for Dark Matter searches*, *JCAP* **03** (2017) 003 [arXiv:1612.06375].

[9] P.A. Amaudruz et al., *Radon backgrounds in the DEAP-1 liquid argon based Dark Matter detector*, *Astropart. Phys.* **62** (2015) 178 [arXiv:1211.0909].

[10] 3M, Inc., *Vikuiti Enhanced Specular Reflector Film*, (2010) https://www.3m.com/3M/en_US/company-us/all-3m-products/~/3M-Enhanced-Specular-Reflector-3M-ESR-/?N=5002385+3293061534&rt=rud.

[11] A. Langenkämper et al., *Low-Temperature Relative Reflectivity Measurements of Reflective and Scintillating Foils used in Rare Event Searches*, *Nucl. Instrum. Meth.* **A 884** (2018) 40 [arXiv:1703.07152].

[12] C.E. Aalseth et al., *DarkSide-20k: A 20 tonne two-phase LAr TPC for direct dark matter detection at LNGS*, *Eur. Phys. J. Plus* **133** (2018) 131.

[13] T. Alexander et al., *The Low-Radioactivity Underground Argon Workshop: A workshop synopsis*, in proceedings of the *Low-Radioactivity Underground Argon*, Richland, Washington, U.S.A., 19–20 March 2018, arXiv:1901.10108v1.

[14] F. Acerbi et al., *Cryogenic Characterization of FBK HD Near-UV Sensitive SiPMs*, *IEEE Trans. Elec. Dev.* **64** (2017) 521.

[15] M. D'Incecco et al., *Development of a Very Low-Noise Cryogenic Preamplifier for Large-Area SiPM Devices*, *IEEE Trans. Nucl. Sci.* **65** (2018) 1005 [arXiv:1706.04213].

[16] W.H. Lippincott et al., *Calibration of liquid argon and neon detectors with $^{83}Kr^m$*, *Phys. Rev.* **C 81** (2010) 045803 [arXiv:0911.5453].

[17] DarkSide collaboration, *Simulation of argon response and light detection in the DarkSide-50 dual phase TPC*, 2017 *JINST* **12** P10015 [arXiv:1707.05630].

[18] J. Allison et al., *Geant4 developments and applications*, *IEEE Trans. Nucl. Sci.* **53** (2006) 270.

[19] ArDM collaboration, *Backgrounds and pulse shape discrimination in the ArDM liquid argon TPC*, *JCAP* **12** (2018) 011 [arXiv:1712.01932].

[20] D.M. Mei, Z.B. Yin, L.C. Stonehill and A. Hime, *A Model of Nuclear Recoil Scintillation Efficiency in Noble Liquids*, *Astropart. Phys.* **30** (2008) 12 [arXiv:0712.2470].